ACS OMEGA

http://pubs.acs.org/journal/acsodf

Article

Effects of the Surface Structure on the Water Transport Behavior in PEMFC Carbon Fiber Papers

Tongqing Qu, Xiyi Huang, and Biao Wang*

Cite This: *ACS Omega* 2022, 7, 5992−5997

Read Online

ACCESS | Metrics & More | Article Recommendations

ABSTRACT: In this paper, three kinds of carbon fiber papers (CFPs), including pure CFP, poly(tetrafluoroethylene) (PTFE)-treated CFP (PTFE-CFP), and microporous layer (MPL)-coated CFP (MPL-CFP), were used to investigate the effects of the surface structure on the water transport behavior in CFPs. Compared to pure CFP, applying PTFE on the CFP increases the breakthrough pressure by 0.2 times, while it decreases the water flow rate at initial penetration by 0.06 times, owing to the strong hydrophobicity of PTFE-CFP. The pore diameter of MPL-CFP reduces sharply after coating the MPL, which leads to increasing breakthrough pressure by 0.6 times. The Young−Laplace equation is applied to study the relationship between the structure (wettability and pore-size distribution) of CFPs and the water transport behavior (breakthrough pressure), and the results show that in addition to wettability and pore size, the pore-size gradient also plays a crucial role in water transport.

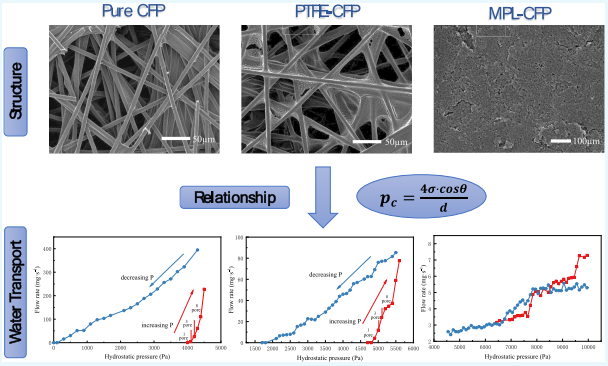

1. INTRODUCTION

The gas diffusion layer (GDL) consisting of carbon fiber papers (CFPs) and the microporous layer (MPL) is a fundamental element of the electrodes in a polymer electrolyte membrane fuel cell (PEMFC).[1] It provides pathways for the product water removal from the catalyst layer (CL) to the flow channel and plays a crucial role in the water management for PEMFC.[2,3] However, excessive amount of liquid water in the GDL blocks the reactant-transporting porous network, hindering oxygen transport to the active sites in the CL and causing mass transport losses.[3,4]

To facilitate removal of water from a GDL and avoid flooding, the CFP in GDL is traditionally treated with PTFE to enhance hydrophobicity or/and coated with the MPL to control the pore structure.[4−7] Bevers et al.[5] studied the influence of PTFE content on the water saturation in CFP, and the results indicated that as the PTFE content increases, the water saturation level decreases. Several other works[6−8] have also numerically demonstrated the situation of saturation reducing with increasing hydrophobicity. Lin et al.[9] provided insight into the effects of the wetproof level of CFP materials on electrode flooding. They concluded that the 20 wt % PTFE treatment prevents liquid water from filling the pores in the hydrophobic region, thereby facilitating good gas transport through the CFP. In addition to the PTFE treatment, a MPL has been applied on the side of the CFP, which contacts with CL to control the pore structure.[2,4] Tabe et al.[10] found that the MPL suppresses water accumulation at the interface owing to the smaller pore size and finer contact with the CL, resulting in less water flooding, which is consistent with the results of Owejan et al.[11] In recent years, several research studies have demonstrated that the incorporation of one-dimensional substances such as carbon nanotubes (CNTs) in the MPL significantly improved the pore structure of the MPL and water management function of PEMFCs.[12−14] The addition of CNTs in the MPL formed hydrophilic large pores, which could enhance the transfer of liquid water from CL to GDL, as more water transfer channels were provided.[13,14] In addition, Mao et al.[15] prepared porous carbon nanofibers (PCNFs) by the electrospinning method and subsequent heat treatment and then built up to form the MPL. The nanosized pores of PCNF and the larger-sized pores formed by the accumulation of PCNF created a pore-size gradient, which accelerated the discharge of the water product from the system because of the capillary effect.

PTFE treatment and MPL coating have proven to be effective methods to improve the water management function of PEMFCs. However, there are a few studies on the relationship between the structure of GDLs and the water transport behavior. Benziger et al.[16,17] introduced water

Received: November 9, 2021
Accepted: January 21, 2022
Published: February 8, 2022

https://doi.org/10.1021/acsomega.1c06304
ACS Omega 2022, 7, 5992−5997

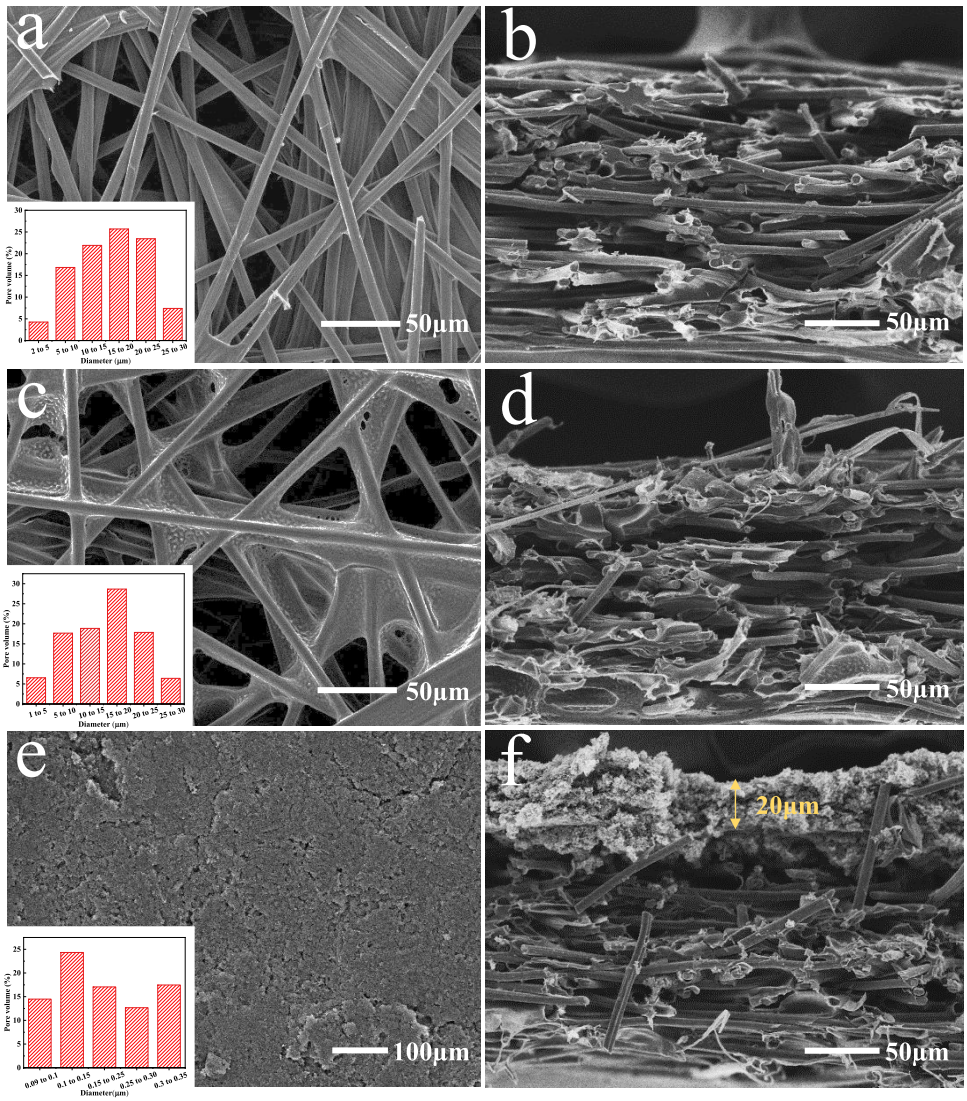

Figure 1. Scanning electron microscopy (SEM) images and pore-size distribution of CFP materials: (a) surface of the CFP; (b) cross section of the CFP; (c) surface of PTFE-CFP; (d) cross section of PTFE-CFP; (e) surface of MPL; and (f) cross section of MPL. The inset in panel (a) is pore-size distribution for CFP, the inset in panel (c) is pore-size distribution for PTFE-CFP, and the inset in panel (e) is pore-size distribution for MPL.

penetration experiments and mathematical models to investigate the water transport behavior in GDL and suggested that liquid water only penetrates a few large pores and the smaller pores remain free of water and allow gas to be transported. Gauthier et al.[1] measured the resistances of transverse and lateral water flow associated with carbon clothes and carbon papers, and the results showed that water flows through the path of least resistance. But they did not study the effects of different surface treatments and structures of CFPs on water transport systematically.

In this paper, the breakthrough pressure, shutoff pressure, and water flow rate for three kinds of commercial CFPs (CFP, PTFE-CFP, and MPL-CFP) were measured and the effects of the surface structure on the water transport behavior were studied. In addition, the mechanism between the structure of CFPs and their water transport behavior was discussed.

2. RESULTS AND DISCUSSION

2.1. Surface Structure Characterization. First of all, the morphology and pore-size distribution of three kinds of CFPs were characterized. As can be seen from Figure 1a, there are three distinct regions including carbon fibers, resin-based carbons, and voids. Long and thin carbon fibers are randomly distributed. These fibers and resin-based carbons are used to transport electrons to and from CL due to their good conductivity. The resin-based carbon region is used to enhance the durability and strength of CFPs, preventing the fibers from cracking.[18] The void region is used as the medium for fluid transport in the gas and/or liquid phase.[18] The pore structure of the CFP is mainly affected by the resin-based carbon content, carbon fiber size, and additives. Since the commercial CFPs used in this experiment are from Toray Industries, the effect of resin-based carbon content and carbon fiber size on the pore structure is negligible. Therefore, the pore size of CFPs is mainly affected by PTFE and MPL. The inset in Figure 1 is the three-dimensional (3D) pore-size distribution for the sample, measured by the aperture analyzer (PMI CFP-1100AI, America). The pore-size distribution of pure CFP is mainly between 2 and 30 μm and conforms to the normal distribution. A cross-sectional morphology is shown in Figure 1b, revealing the configuration of carbon fibers in the through-plane direction. Carbon fibers are bonded together by resin-

https://doi.org/10.1021/acsomega.1c06304
ACS Omega 2022, 7, 5992−5997

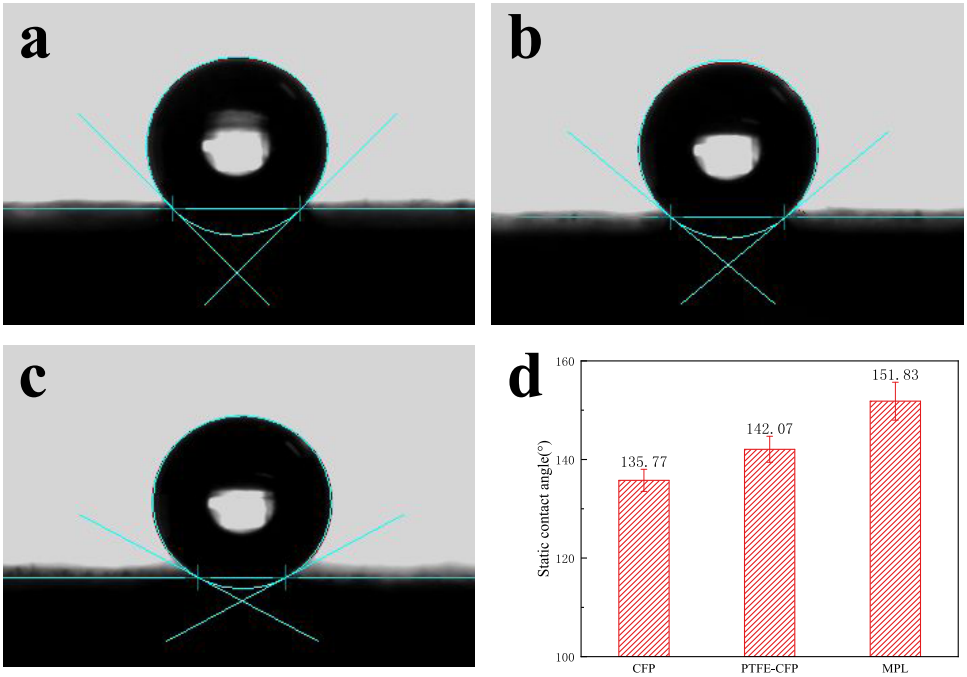

Figure 2. Static contact angle of CFP materials: (a) CFP; (b) PTFE-CFP; and (c) MPL. (d) Graphical comparison of the average contact angles of panels (a)−(c).

based carbons and the pores are interconnected and penetrated.

Compared to pure CFP, the structure of the binding materials (resin-based carbons) of PTFE-CFP has some changes as shown in Figure 1c. Due to the presence of PTFE, the pore size of PTFE-CFP is slightly smaller but the pore-size distribution still conforms to the normal distribution. The morphology of the MPL is shown in Figure 1e, and the CFP surface is covered by powdery layers, resulting in tiny pore structures.[19] The micropores are situated among the carbon black aggregates and agglomerations,[20] having a size between 0.09 and 0.35 μm. The pore-size distribution of the MPL is relatively uniform, so as to better contact with the CL. The thickness of the MPL is ∼20 μm, which can be observed from Figure 1f. These pore structures of CFPs not only have an impact on the matching of CL but also play an important role in water transport.

Figure 2 displays images of the static water contact angle measurement of CFPs. The average contact angles of CFP, PTFE-CFP, and MPL are 135.77, 142.07, and 151.83°, respectively. After the PTFE treatment, the contact angle of the CFP has been significantly improved, which means that the PTFE treatment makes the CFP more hydrophobic. PTFE was introduced into the CFP by dipping, so it could ensure that the pores inside PTFE-CFP and MPL-CFP were also hydrophobic. It is well known that both surface energy and surface morphology play important roles in contact angle.[19,21] Both PTFE-CFP and MPL have been subjected to hydrophobic treatment, so their surface energy is low. In addition, the MPL is composed of carbon particles and has a small pore size (inset in Figure 1e); this microstructure limits the water infiltration, so the MPL is more hydrophobic.[22]

2.2. Transverse Water Penetration. The drainage process of liquid water through the CFP can be regarded as a process in which the nonwetting fluid (water) replaces the wetting fluid (gas), so this experiment was conducted in the two-phase flow regime.[1] Figure 3 shows the average mass flow rate as a function of hydrostatic pressure. A series of vertical lines are shown and indicate the number of different drops seen on the surface of the CFP sample. The flow rates increase as the number of drops increase and also increase at some points where no new drops are observed. At these points, one drop appears to grow and detach at a faster rate than before.[1] The hydrostatic pressure is increased until 8−10 drops are formed simultaneously, and then the pressure is stepped down until the flow of water ceases.

The data in Figure 3a,3b are obtained from the CFP and PTFE-CFP samples. The breakthrough processes are similar, but the breakthrough pressure, shutoff pressure, and flow rate show some variability, reflecting different wettability and pore sizes between samples. The breakthrough pressures for CFP and PTFE-CFP are 4100 and 4900 Pa, respectively, showing that applying PTFE on the CFP increases the breakthrough pressure by 0.2 times. According to the Young−Laplace equation[23] in eq 1, the surface wettability and pore structure of CFPs have great impacts on the capillary resistance, which is relative to the breakthrough pressure

$$p_c = \frac{4\sigma \cdot \cos\theta}{d} \quad (1)$$

where p_c is the capillary resistance; σ is the surface tension, 71.97 × 10^{-3} N/m; θ is the contact angle, and d is the diameter of capillary channels.

For simplicity, we assume that the pores are cylindrical and run transverse across the CFP,[16] and the maximum pore diameters of CFP and PTFE-CFP are both 30 μm (inset in Figure 1). The breakthrough pressure should be slightly greater than the capillary resistance. Substituting the contact angle in Figure 2d in eq 1, the calculated capillary resistance values for CFP and PTFE-CFP are 6876 and 7569 Pa, respectively. Since there may be pores larger than 30 μm in CFP, the calculated results are larger than the experimental results but their trends

https://doi.org/10.1021/acsomega.1c06304
ACS Omega 2022, 7, 5992−5997

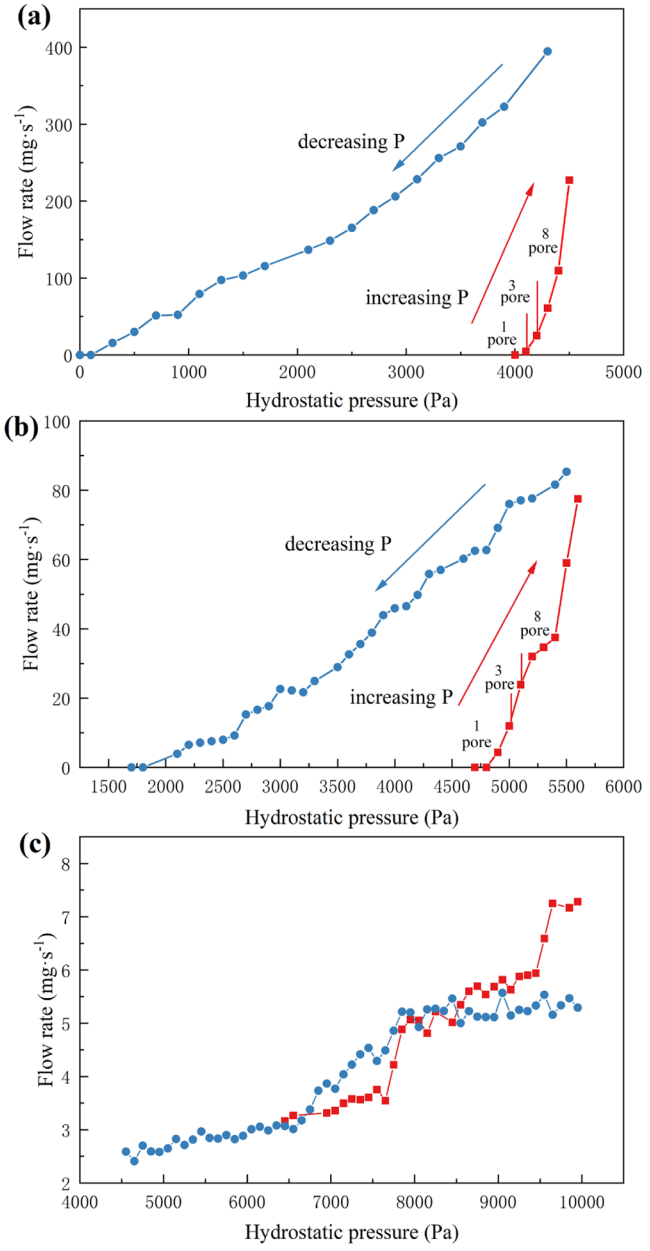

Figure 3. Penetration of water through CFPs: (a) CFP; (b) PTFE-CFP; and (c) MPL-CFP. The arrows designate the direction of pressure change. Trial 1 (red line) is for the MPL-CFP sample initially fully dried. Trial 2 (blue line) is water penetration for the same sample after the initial water penetration from Trial 1.

are consistent. In addition, the water flow rates at initial penetration for CFP and PTFE-CFP are 4.65 and 4.35 mg/s, which means that the PTFE treatment makes the flow rate decrease.[2]

Figure 3c shows the water flow rate through MPL-CFP as a function of hydrostatic pressure. Trial 1 (red line) is for the MPL-CFP sample initially fully dried. Trial 2 (blue line) is water penetration for the same sample after the initial water penetration from Trial 1.[1] The breakthrough pressure for MPL-CFP is 6450 Pa, which shows that applying the MPL increases the breakthrough pressure by 0.6 times owing to the diminutive size of MPL pores, creating greater capillary resistance. According to eq 1, the calculated capillary resistance of MPL-CFP is 725 088 Pa, which is far greater than the breakthrough pressure for CFP. We suggest that the reason why the calculated capillary resistance is much higher than the experimental result may be the destruction of the MPL structure by water penetration. Therefore, the MPL promotes the back-diffusion of water, leading to difficulty in water removal.

In addition, only one drop is observed on the surface of the MPL-CFP sample during the whole penetration process. We suggest that the cracks or large pores in the MPL provide a water flow channel and permit sustained water removal. Inspired by these phenomena, we can introduce hydrophilic components into the MPL to form a hydrophilic channel, which can not only reduce the breakthrough pressure but also control the water flow.

The shutoff pressure decreases compared with the initial breakthrough pressure. We suggest that a small amount of residual water remains attached in the porous CFP and this water reduces the capillary resistance that water needs to overcome to penetrate the CFP. Previous research showed that water saturation in the CFP was considerably decreased after the PTFE treatment and introduction of MPL.[2] After the initial water penetration, the water saturation in pure CFP is higher, and the capillary resistance that water needs to overcome to penetrate the CFP is lower, so the shutoff pressure is lower. However, the water saturation in PTFE-CFP and MPL-CFP is still low, so they require a higher shutoff pressure to permit sustained water removal.

The effect of the pore-size gradient on water transport was also explored. The MPL measured above was at the top, and the water passed through the MPL first and then through the CFP. Here, the location of the MPL was changed from top to bottom by reversing the direction of MPL-CFP; thereby, the water passed through the CFP with large pores first and then the MPL. The water penetration experiment was conducted under the same conditions mentioned above. The results in Figure 4 show that the breakthrough pressure increases by 0.2

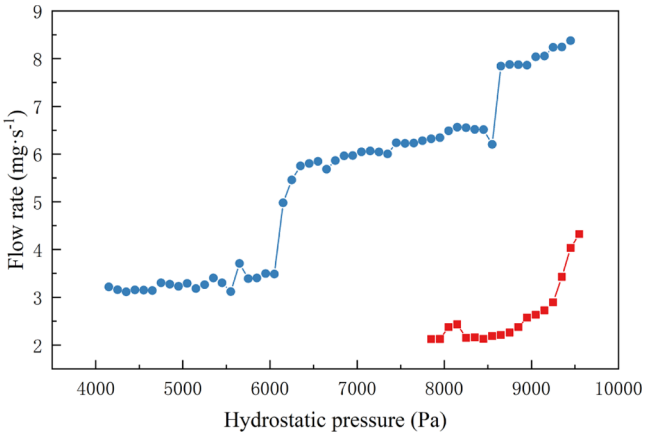

Figure 4. Penetration of water through MPL-CFP when the MPL is at the bottom.

times and the water flow rate slightly decreases when the MPL is at the bottom. It is confirmed that in hydrophobic CFPs, water tends to flow from small pores to large pores.

There is a simple physical penetration model used to explain these phenomena.[24] The water states in MPL-CFPs are shown in Figure 5, the pore diameters of MPL and CFP are d_1 and d_2, respectively ($d_1 < d_2$). Such a composite porous structure

https://doi.org/10.1021/acsomega.1c06304
ACS Omega 2022, 7, 5992−5997

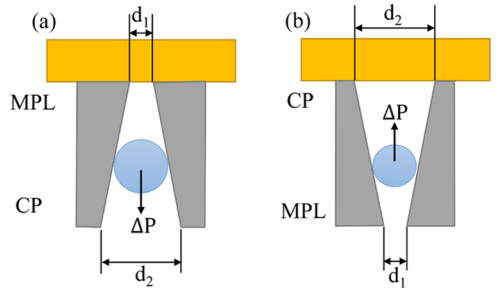

Figure 5. Water states of different positions of MPL: (a) MPL is at the top and (b) MPL is at the bottom.

generates a superposed capillary pressure difference (ΔP) from two kinds of pores as follows[23]

$$\Delta P = \frac{4\sigma\cdot\cos\theta_1}{d_1} - \frac{4\sigma\cdot\cos\theta_2}{d_2} \quad (2)$$

where σ is the surface tension, 71.97×10^{-3} N/m; θ is the contact angle; and d is the diameter of capillary channels.

The pore size (inset in Figure 1) of the MPL is significantly smaller than that of the CFP and the contact angle (Figure 2d) of the MPL is greater than that of the CFP. Thus, the capillary pressure of the MPL (P_{C1}) is much larger than that of the CFP (P_{C2}). When the MPL is at the top, the ΔP will promote water transmission, thereby reducing the breakthrough pressure. However, when the MPL is at the bottom, the ΔP will inhibit water transport, thus increasing the breakthrough pressure. This model also verifies the accuracy of the results shown in Figures 3c and 4. Therefore, we can design and fabricate tailored CFPs with a pore-size gradient (increasing from CL to the flow channel) to enhance the water removal in PEMFC.

Table 1 summarizes the breakthrough pressure, shutoff pressure, and flow rate at initial penetration for different CFP materials. The shutoff pressure represents the minimum pressure differential between the cathode CL and the flow channel to permit sustained water removal from the CL.[1] If the pressure differential is below the shutoff pressure, the liquid flow will stop and the pressure differential must build up to exceed the shutoff pressure for water flow to recommence.[1] During the operation of the fuel cell, water breaking through the CFP for the first time needs to overcome a higher pressure. Once a pore is broken through, the water pressure only needs to exceed the shutoff pressure for the flow to continue.

Table 1. Breakthrough, Shutoff, and Flow through CFP Materials

CFP materials	breakthrough pressure (Pa)	shutoff pressure (Pa)	flow rate at initial penetration (mg/s)
pure CFP	4100	100	4.65
PTFE-CFP	4900	1800	4.35
MPL-CFP (top)	6450	4550	3.17
MPL-CFP (bottom)	7850	4150	2.12

3. CONCLUSIONS

Changing the CFP surface wettability to more hydrophobic creates greater capillary resistance for liquid water to penetrate the pores of PTFE-CFP. The diminutive size of MPL pores creates larger capillary resistance, so that liquid water requires quite higher pressure to pass through MPL-CFP. The cracks or large pores in the MPL could provide a water flow channel and permit sustained water removal. The pore-size gradient also has significant impacts on the water transport behavior and water is more inclined to flow from small pores to large pores because of the capillary pressure difference.

4. MATERIALS AND METHODS

4.1. Materials. Pure CFP (TGP-H-060) with a thickness of 190 μm and PTFE-CFP (15 wt % PTFE emulsion-treated TGP-H-060 CFP) were purchased from SUZHOU SINERO TECHNOLOGY CO. MPL-CFP (MPL-coated TGP-H-060 CFP) with a thickness of 210 μm was supplied by JUNJIKEJI CO.

4.2. Physical and Morphological Characterization. The morphology of the samples was observed by scanning electron microscopy (SEM, JSM-IT300, Japan). The surface wettability of samples was tested using a contact angle meter (OCA40Mircro, Germany). The pore-size distribution and pore volume of CFPs were determined using an aperture analyzer (PMI CFP-1100AI, America), which is a 3D measurement.

4.3. Transverse Transport Experiments. A cell similar to that used by Gauthier et al.[1] was applied to measure the transverse liquid water transport shown in Figure 6. A sample of CFP was placed between two chambers. One of the chambers was filled with liquid water and connected to a water reservoir through a tygon tube; the other side was kept at an atmospheric pressure and allowed water to drain directly into a beaker on the analytical balance (FA2204N, China). The piece of the CFP exposed to water was 2.5 cm in diameter (total area of ~5 cm^2). CFPs were stored in desiccators prior to testing. The water pressure on the CFP was controlled by changing the height of the liquid water in the water reservoir. The hydrostatic pressure of liquid water was increased incrementally by 1 cm water (100 Pa) every 30 s. The mass of water passing through the CFP was recorded every 30 s. The CFP surface was visible through an acrylic plate, and the number of drops forming on the surface of the CFP sample was recorded at each hydrostatic pressure. The pressure measurements are accurate to ±10 Pa. Although there were differences between different samples taken from the same CFP sample, which is a

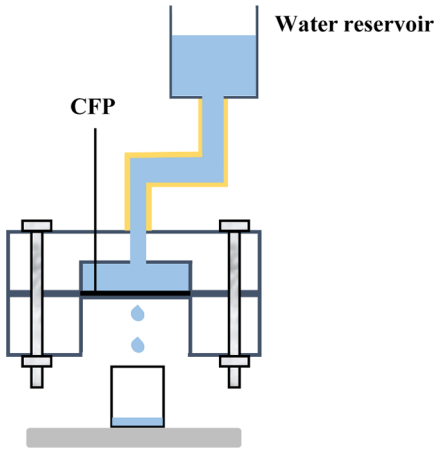

Figure 6. Experimental system for water penetration and flow rate measurements.

https://doi.org/10.1021/acsomega.1c06304
ACS Omega 2022, 7, 5992−5997

consequence of the tail of the pore-size distribution, the overall trend was the same.

AUTHOR INFORMATION

Corresponding Author

Biao Wang − *State Key Laboratory for Modification of Chemical Fibers and Polymer Materials, College of Materials Science and Engineering, Donghua University, Shanghai 201620, P. R. China*; Email: wbiao2000@dhu.edu.cn

Authors

Tongqing Qu − *State Key Laboratory for Modification of Chemical Fibers and Polymer Materials, College of Materials Science and Engineering, Donghua University, Shanghai 201620, P. R. China*; orcid.org/0000-0002-9895-7446

Xiyi Huang − *State Key Laboratory for Modification of Chemical Fibers and Polymer Materials, College of Materials Science and Engineering, Donghua University, Shanghai 201620, P. R. China*

Complete contact information is available at: https://pubs.acs.org/10.1021/acsomega.1c06304

Notes

The authors declare no competing financial interest.

ACKNOWLEDGMENTS

This work was financially supported by the National Key R&D Program of China (Grant No. 2020YFB15057000).

REFERENCES

(1) Gauthier, E.; Duan, Q.; Hellstern, T.; Benziger, J. Water Flow in, Through, and Around the Gas Diffusion Layer. *Fuel Cells* **2012**, *12*, 835−847.

(2) Jinuntuya, F.; Kamsanam, W. Effects of Structure and Hydrophobic Treatment on Water Transport Behaviour in PEM Fuel Cell Gas Diffusion Layers. *IOP Conf. Ser.: Mater. Sci. Eng.* **2019**, *501*, No. 012051.

(3) Sinha, P. K.; Mukherjee, P. P.; Wang, C.-Y. Impact of GDL structure and wettability on water management in polymer electrolyte fuel cells. *J. Mater. Chem.* **2007**, *17*, 3089−3103.

(4) Ferreira, R. B.; Falcao, D. S.; Oliveira, V. B.; Pinto, A. Experimental study on the membrane electrode assembly of a proton exchange membrane fuel cell: effects of microporous layer, membrane thickness and gas diffusion layer hydrophobic treatment. *Electrochim. Acta* **2017**, *224*, 337−345.

(5) Bevers, D.; Rogers, R.; vonBradke, M. Examination of the influence of PTFE coating on the properties of carbon paper in polymer electrolyte fuel cells. *J. Power Sources* **1996**, *63*, 193−201.

(6) Chapuis, O.; Prat, M.; Quintard, M.; Chane-Kane, E.; Guillot, O.; Mayer, N. Two-phase flow and evaporation in model fibrous media - Application to the gas diffusion layer of PEM fuel cells. *J. Power Sources* **2008**, *178*, 258−268.

(7) Hao, L.; Cheng, P. Lattice Boltzmann simulations of water transport in gas diffusion layer of a polymer electrolyte membrane fuel cell. *J. Power Sources* **2010**, *195*, 3870−3881.

(8) Jinuntuya, F.; Whiteley, M.; Chen, R.; Fly, A. The effects of gas diffusion layers structure on water transportation using X-ray computed tomography based Lattice Boltzmann method. *J. Power Sources* **2018**, *378*, 53−65.

(9) Lin, G. Y.; Van Nguyen, T. Effect of thickness and hydrophobic polymer content of the gas diffusion layer on electrode flooding level in a PEMFC. *J. Electrochem. Soc.* **2005**, *152*, A1942−A1948.

(10) Tabe, Y.; Aoyama, Y.; Kadowaki, K.; Suzuki, K.; Chikahisa, T. Impact of micro-porous layer on liquid water distribution at the catalyst layer interface and cell performance in a polymer electrolyte membrane fuel cell. *J. Power Sources* **2015**, *287*, 422−430.

(11) Owejan, J. P.; Owejan, J. E.; Gu, W. B.; Trabold, T. A.; Tighe, T. W.; Mathias, M. F. Water Transport Mechanisms in PEMFC Gas Diffusion Layers. *J. Electrochem. Soc.* **2010**, *157*, B1456−B1464.

(12) Jung, G. B.; Tzeng, W. J.; Jao, T. C.; Liu, Y. H.; Yeh, C. C. Investigation of porous carbon and carbon nanotube layer for proton exchange membrane fuel cells. *Appl. Energy* **2013**, *101*, 457−464.

(13) Lin, R.; Tang, S. H.; Diao, X. Y.; Zhong, D.; Chen, L.; Froning, D.; Hao, Z. X. Detailed optimization of multiwall carbon nanotubes doped microporous layer in polymer electrolyte membrane fuel cells for enhanced performance. *Appl. Energy* **2020**, *274*, No. 115214.

(14) Kitahara, T.; Nakajima, H.; Okamura, K. Gas diffusion layers coated with a microporous layer containing hydrophilic carbon nanotubes for performance enhancement of polymer electrolyte fuel cells under both low and high humidity conditions. *J. Power Sources* **2015**, *283*, 115−124.

(15) Mao, L. C.; Jin, J. H.; Yang, S. L.; Li, G. Performance of porous carbon nanofibers as microporous layer for proton exchange membrane fuel cells. *Chem. Ind. Eng. Prog.* **2020**, *39*, 3995−4001.

(16) Benziger, J.; Nehlsen, J.; Blackwell, D.; Brennan, T.; Itescu, J. Water flow in the gas diffusion layer of PEM fuel cells. *J. Membr. Sci.* **2005**, *261*, 98−106.

(17) Kimball, E.; Whitaker, T.; Kevrekidis, Y. G.; Benziger, J. B. Drops, slugs, and flooding in polymer electrolyte membrane fuel cells. *AIChE J.* **2008**, *54*, 1313−1332.

(18) Zamel, N.; Li, X. G.; Shen, J. Correlation for the Effective Gas Diffusion Coefficient in Carbon Paper Diffusion Media. *Energy Fuels* **2009**, *23*, 6070−6078.

(19) Yoshimune, W.; Kato, S.; Yamaguchi, S.; Akimoto, Y.; Koiwai, A.; Nakamura, H. Managing the Pore Morphologies of Microporous Layers for Polymer Electrolyte Fuel Cells with a Solvent-Free Coating Technique. *ACS Sustainable Chem. Eng.* **2021**, *9*, 7922−7929.

(20) Chen, J.; Matsuura, T.; Hori, M. Novel gas diffusion layer with water management function for PEMFC. *J. Power Sources* **2004**, *131*, 155−161.

(21) Bhushan, B.; Jung, Y. C. Natural and biomimetic artificial surfaces for superhydrophobicity, self-cleaning, low adhesion, and drag reduction. *Prog. Mater. Sci.* **2011**, *56*, 1−108.

(22) Li, H.; Yan, T. Y.; Fichthorn, K. A.; Yu, S. R. Dynamic Contact Angles and Mechanisms of Motion of Water Droplets Moving on Nanopillared Superhydrophobic Surfaces: A Molecular Dynamics Simulation Study. *Langmuir* **2018**, *34*, 9917−9926.

(23) Wang, X. F.; Huang, Z.; Miao, D. Y.; Zhao, J.; Yu, J. Y.; Ding, B. Biomimetic Fibrous Murray Membranes with Ultrafast Water Transport and Evaporation for Smart Moisture-Wicking Fabrics. *ACS Nano* **2019**, *13*, 1060−1070.

(24) Tang, H. L.; Wang, S. L.; Pan, M.; Yuan, R. Z. Porosity-graded micro-porous layers for polymer electrolyte membrane fuel cells. *J. Power Sources* **2007**, *166*, 41−46.